

Toward the Detection of Cyanoketene in the Interstellar Medium: New Hints from Quantum Chemistry and Rotational Spectroscopy

Bernardo Ballotta,* Tainah D. Marforio, Sergio Rampino, Emilio Martínez-Núñez, Vincenzo Barone, Mattia Melosso, Andrea Bottoni, and Luca Dore*



Cite This: *ACS Earth Space Chem.* 2023, 7, 1172–1180



Read Online

ACCESS |



Metrics & More



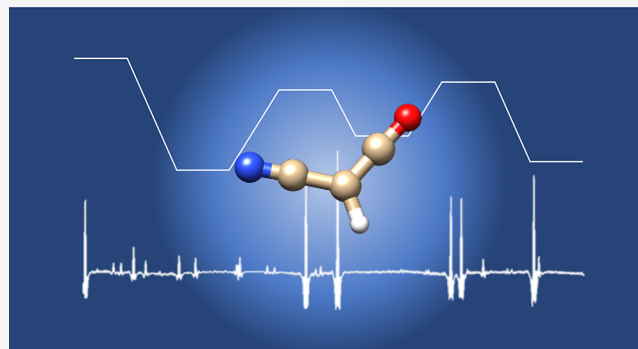
Article Recommendations



Supporting Information

ABSTRACT: A detailed quantum chemical investigation of a new reaction mechanism possibly leading to the formation of cyanoketene (NC-CH=C=O) in the interstellar medium (ISM) was carried out. Different reaction channels have been found by the AutoMeKin program, and the structures and harmonic force fields of the key stationary points have been characterized at the density functional theory level employing last-generation double-hybrid functionals. Finally, single-point computations at those geometries by state-of-the-art composite wave function methods provided accurate energies for the evaluation of thermochemical and kinetic parameters in the framework of an *Ab Initio* Transition State Theory based Master Equation (AITSTME) strategy. Our results indicate that the barrier-less association reaction of the formyl radical (HCO^\bullet) to the cyanocarbene radical (HCCN) can lead to the formation of cyanoketene under the harsh conditions of the ISM. Canonical rate constants computed for temperatures up to 600 K show that the most abundant product is indeed cyanoketene. The formation of other, even more stable, species involves higher activation energies and/or less favorable multi-step processes. Furthermore, to aid the search of cyanoketene, still undetected in the ISM, its rotational spectrum was recorded up to 530 GHz. The refined set of spectroscopic constants obtained in this way allows for spectral predictions from the microwave to the terahertz region, particularly for the bright b-type transitions, which can be targeted for the identification of cyanoketene in spectral line surveys. Despite cyanoketene was already sought without success in a variety of astronomical sources, we suggest to look for it in those sources where HCO or HCCN have already been detected, namely, W3, NGC2024, W51, K3-50, IRC + 2016, and TMC-1.

KEYWORDS: astrochemistry, interstellar species, cyanoketene, rotational spectroscopy, quantum chemistry, kinetics



1. INTRODUCTION

A recent joint laboratory–observational paper¹ addressed the issue of the presence of cyanoketene (NC-CH=C=O) in the interstellar medium (ISM). The rationale for the search of this molecule was the 44-year-old detection of ketene ($\text{H}_2\text{C=C=O}$)² and the existence of several CN-containing molecules in the ISM,³ such as cyanoformaldehyde,⁴ aminoacetonitrile,^{5,6} benzonitrile,⁷ and many cyanopolynes.^{8–11} Searched for in several star-forming regions, cyanoketene was not detected, and its chemical formation route was discussed by Margulès et al., who suggested three possible pathways: (i) the addition of the CN radical to ketene or (ii) to the ketylenyl radical (H-C=C=O) and (iii) the reaction of the C_3N radical with water. While the third reaction would probably lead to different products,¹ the first two reactions represent plausible formation pathways for cyanoketene in the ISM. Indeed, the reaction between the CN radical and a neutral partner has already been shown to be an effective formation route for some other molecules in the ISM (see, e.g., Vazart et al.¹² for

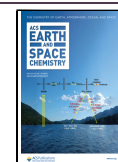
cyanomethanimine and Tonolo et al.¹³ for cyanoformaldehyde). Anyway, computational and experimental studies for the addition of CN to ketene by Zhang and Du, Sun et al., and Edwards and Hershberger^{14–16} showed that this reaction leads to the formation of $\text{CO} + \text{H}_2\text{C}_2\text{N}$ through a dissociative recombination process. Because reaction ii is a radiative association process, the final product is expected to be stabilized by photon emission; otherwise, the excess energy would lead to back dissociation to the initial reactants, as already proposed in the case of the formation cyanoacetaldehyde.¹⁷ For this reason, Margulès et al. considered this reaction unlikely in the ISM but possible on grain surfaces. Finally, a

Received: March 6, 2023

Revised: April 1, 2023

Accepted: April 3, 2023

Published: April 12, 2023



computational investigation of reaction iii by Xie et al.¹⁸ showed that it cannot occur at very low temperatures because of a non-negligible energy barrier for the hydrogen abstraction. The same authors also studied the catalytic effect of water on the reaction and found that, with the increase of the number of catalyzing water molecules, the reaction becomes barrierless. However, as a result of the very low pressure characterizing the ISM, reactions between more than two reactants are very unlikely; thus, this reaction channel does not seem plausible for cyanoketene synthesis.

In addition to these possibilities, a computational study of Xie et al.¹⁹ found NCCHCO as an intermediate of the reaction between atomic oxygen and cyanoacetylene (HC_3N) in the gas phase and on water ice. By investigation of both gas-phase- and water-ice-catalyzed reactivity, it was shown that the activation energy governing the gas-phase process can be strongly lowered by the catalytic activity of water, up to producing a barrierless process. Another mechanism, involving the reaction between NCO and C_2H_2 , was proposed by Xie et al.²⁰ and leads to cyanoketene as one of the possible products. Unfortunately, this process involves a non-negligible energy barrier, which cannot be overcome under the ISM conditions. Furthermore, the authors performed a kinetic analysis, and the result demonstrated that the preferred products are HCN and HC_2O .

In the present work, we suggest an alternative mechanism for the formation of cyanoketene, which involves two reactants already detected in the ISM, namely, the cyanocarbene (HCCN)²¹ and formyl (HCO)²² radicals. To obtain an accurate description of reaction energies and activation barriers, a full quantum mechanical investigation of different reaction paths has been carried out combining state-of-the-art density functionals and wave function composite methods.²³ Exploiting these data, a kinetic analysis has next been performed employing a master equation (ME) approach to compute the formation rate constants of the products and to prove the effectiveness of the mechanism proposed.

Additionally, we have extended the study of the rotational spectrum of cyanoketene into the submillimeter-wave range to facilitate its astronomical observation. Although most of the first interstellar detections relied on low-frequency observations,³ the higher frequency spectral windows covered by modern facilities [such as Atacama Large Millimeter/Submillimeter Array (ALMA) or Stratospheric Observatory for Infrared Astronomy (SOFIA)] offer further chances to detect additional complex organic molecules (COMs), i.e., molecules containing at least one carbon atom and a total of at least six atoms. Their capabilities have been demonstrated recently by the discovery of interstellar species (including COMs) observable only in the terahertz (THz) domain^{24–26} by exploiting high-frequency ALMA band 10 spectral line surveys.^{27,28}

Based on these premises, the rotational spectrum of cyanoketene has been measured up to 530 GHz, with the inclusion of additional *b*-type Q branch transitions with respect to the data reported by Margulès et al.¹ These improvements allowed for a refinement of all of the spectroscopic constants and a precise determination of the purely K_a -dependent centrifugal distortion constants up to the eighth order. On the whole, the newly determined set of spectroscopic parameters extends the range of reliable spectral predictions up to the ALMA band 9 (602–720 GHz).

2. COMPUTATIONAL DETAILS

2.1. Reaction Mechanism Discovery. Feasible reaction paths have been generated by means of the AutoMeKin^{29–31} program, designed for the automated reaction mechanism discovery. The program is based on the application of methods and concepts rooted in graph theory, reactive molecular dynamics, and electronic structure. The dynamic simulations needed to obtain the initial structures of the transition states (TSs) governing putative reaction mechanisms were performed using the semi-empirical PM7 method³² implemented in the MOPAC package.³³ A total of 100 trajectories per iteration (keyword *ntraj*) were calculated for a total of 10 iterations. The screening parameters used to avoid redundant structures included a value of 100 cm^{-1} for the smallest accepted imaginary frequency (keyword *imagmin*) to also take into account torsional transition states and a value of 0.1 for the lowest eigenvalue of the Laplacian used to differentiate the structures resulting from the fragmentation of an intermediate (keyword *eigLmax*). Two other parameters (MAPEmax and BAPEmax) used to compare the descriptors characterizing the different structures obtained from the molecular dynamics simulations were set to 0.002 and 1.5, respectively. Further details about these screening parameters can be found in ref 37. After this step, optimized geometries and zero-point-corrected electronic energies of reactants, transition states, intermediates, and products along the reaction pathways were obtained by the rev-DSD-PBEP86³⁴-GD3BJ³⁵ double-hybrid functional in conjunction with the jun-cc-pVTZ basis set.³⁶ This combination of functional and basis set will be referred to in the following as rDSD.

Diagonalization of analytical rDSD Hessians³⁷ allowed also to characterize all of the critical points belonging to the reaction pathways as minima (reactants, intermediates, and products) and saddle points (TSs). The different elementary steps were further characterized following rDSD intrinsic reaction coordinates (IRCs)³⁸ starting from the different TSs.

The results of the simulations have been analyzed using the AMK tool,³⁹ which allows for the examination of the extremely complex reaction networks generated by AutoMeKin, by visualizing molecular structures with their vibrational normal modes and checking the potential energy profiles of the reaction mechanisms investigated. Thanks to AMK, it has been possible to find the reaction pathways that lead to the formation of cyanoketene and to select the structures of all of the critical points ruling these paths. For such structures, improved electronic energies were obtained by single-point computations exploiting the junChS-F12 composite scheme described in more detail in the next subsection.

2.2. junChS-F12 Composite Scheme. It is well-known that for systems not showing strong multireference character the coupled-cluster (CC) model including single, double, and perturbative estimates of triple excitations [$\text{CCSD}(\text{T})$]⁴⁰ delivers accurate electronic energies provided that complete basis set (CBS) extrapolation and core valence (CV) correlation are properly taken into account. The key idea of the reduced cost cheap scheme (ChS)^{23,41–43} is that, starting from frozen core (fc) $\text{CCSD}(\text{T})$ computations in conjunction with a (partially augmented) triple- ζ basis set,^{44–47} CBS and CV terms can be computed with good accuracy and negligible additional cost employing the second-order Møller–Plesset perturbation theory (MP2).⁴⁸ In particular, the CBS extrapolation by the standard n^{-3} two-point formula⁴⁹ employs

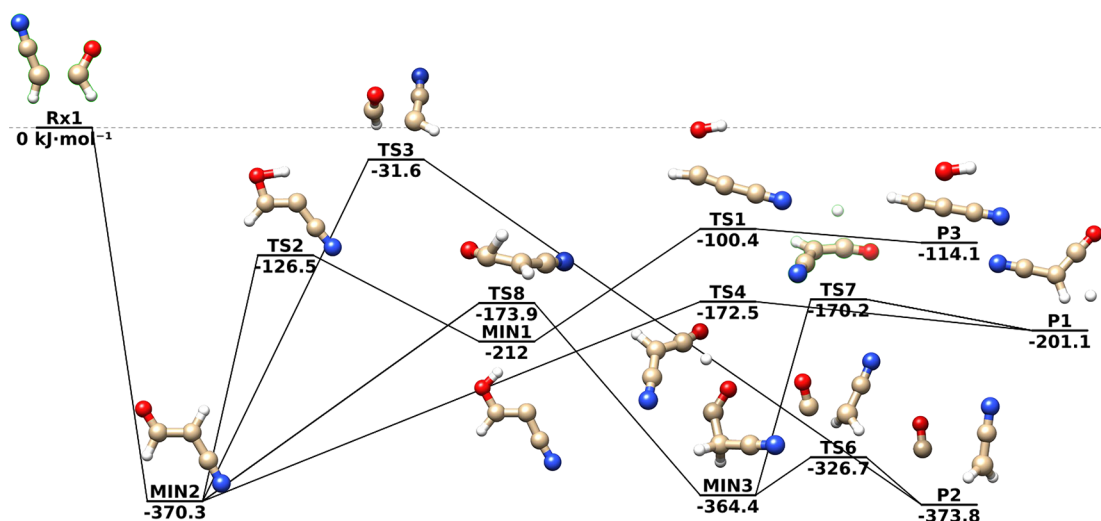


Figure 1. Energetics of the reaction: junChS-F12 electronic energies augmented by rDSD anharmonic ZPE corrections. Energies are in kJ mol^{-1} relative to the reactant limit.

MP2/jun-cc-pV(X+d)Z energies with $X = T$ and Q , whereas the CV contribution is incorporated as the difference between all-electron (ae) and fc MP2 calculations, both with the cc-pCVW(T+d)Z basis set.⁵⁰ Replacement of conventional methods by the explicitly correlated (F12) variants^{51,52} leads to our current standard version of the approach, which is referred to as junChS-F12.^{53–55} A comparison to the most accurate results available for reaction energies and activation barriers^{23,53,55} showed that junChS-F12 energy evaluations at rDSD optimized geometries provide average absolute errors of the order of 1 kJ mol^{-1} . Therefore, this approach was employed for all of the stationary points in conjunction with anharmonic zero-point vibrational energy corrections computed in the framework of the second-order vibrational perturbation theory⁵⁶ employing rDSD anharmonic force fields.

All density functional theory (DFT) calculations were performed using Gaussian16,⁵⁷ while junChS-F12 calculations were performed using MOLPRO.^{58–60}

2.3. Kinetics. Global and channel-specific rate constants have been computed in the framework of the *Ab Initio* Transition State Theory based Master Equation (AITSTME) approach employing the MESS software⁶¹ to solve the multi-well one-dimensional master equation by the chemically significant eigenvalue (CSE) method. The collisional energy transfer probability is described using the exponential down model⁶² with a temperature-dependent $\langle \Delta E_{\text{down}} \rangle$ of $260(T/298)^{0.875} \text{ cm}^{-1}$ in an argon bath.

For elementary steps governed by distinct saddle points, rate coefficients are determined by the conventional transition state theory (TST) within the rigid-rotor harmonic-oscillator (RRHO) approximation and including tunneling as well as non-classical reflection effects using the Eckart model.⁶³

Instead, rate constants for barrierless elementary reactions are computed employing the phase space theory (PST).^{64,65} The long-range interaction between the incoming reactants is described by an isotropic attractive potential $V(R) = -C_6/R^6$.⁶⁶ The C_6 parameter ($90.12a_0^6 E_h$) has been obtained by a least squares fitting of rDSD electronic energies computed at different values of the HOC–CHCN distance. It is well-known that PST can overestimate the rate constant of barrierless association reactions leading to uncertainties of up to a factor

of 2–3 on the total reaction rates with respect to experimental data and/or theoretical estimations obtained by more sophisticated methods.^{67,68} However, the main aim of our work is to provide a semi-quantitative support to the suggested reaction mechanism. In this context, the above-mentioned uncertainty does not impair the comparison between different products because the entrance channel is common to all of them. This comment does not detract, of course, from the possibility of applying in forthcoming studies more elaborate methods, which have proven to be more reliable in the quantitative determination of the reaction rate constants.

Rate constants have been evaluated for a pressure of 1×10^{-8} bar in the 10–600 K temperature range to mimic the typical conditions of different regions of the ISM. Next, the rate constants at different temperatures have been fitted to a three-parameter-modified Arrhenius equation, namely, the Arrhenius–Kooij expression^{69,70}

$$k(T) = A \left(\frac{T}{300} \right)^n e^{-E/RT}$$

where A , n , and E are the fitting parameters and R is the universal gas constant.

The key results of the kinetic analysis have been further checked by computations performed with the StarRate program, specifically designed for reactions of astrochemical interest.^{71,72}

3. POTENTIAL ENERGY SURFACE (PES)

A schematic diagram of the PES generated by AutoMeKin is shown in Figure 1. The initial reactants, Rx1, are the HCO and HCCN radicals, whose electronic ground states are a doublet and a triplet, respectively. In analogy with the formation route of ethanimine investigated by Balucani et al.⁷³ and Baiano et al.,⁷⁴ a total of six spin states are thus possible, including the two components of the reactive doublet state, which can bring the formation of a chemical bond and the four components of the non-reactive quartet state.

3.1. Description of the Reaction Mechanism. We recall that both the reactants representing the asymptotic limit (AL), namely, HCCN (triplet state) and HCO (doublet state), have been detected in the ISM. As shown in Figure 2, the formyl

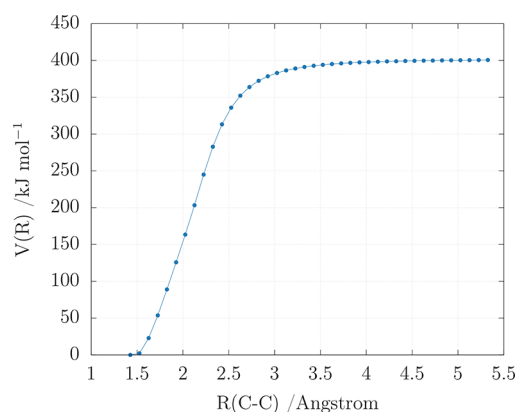


Figure 2. One-dimensional potential energy profile as a function of C–C bond formation (Å) for the reaction of $\text{HCCN} + \text{HCO} \rightarrow \text{MIN2}$ computed at the rDSD level.

radical carries out a barrierless attack on sp^2 carbon of the cyanocarbene radical, which brings the formation of the new C–C bond and leads to a strong stabilization of the system. The intermediate reached at the end of this step (MIN2) lies $370.3 \text{ kJ mol}^{-1}$ below the AL. MIN2 can next undergo a hydrogen transposition, which leads to the formation of another (less stable) reaction intermediate MIN1 and, subsequently, through the breaking of the C–O bond, leads to the P3 products, i.e., cyanoacetylene (HC_3N) and the hydroxyl radical (OH).

Another reactive pathway that can originate from MIN2 is the dissociation with the simultaneous hydrogen transfer reaction leading to the formation of P2 at $-373.8 \text{ kJ mol}^{-1}$, i.e., carbon monoxide (CO) and the cyanomethyl radical ($\text{H}_2\text{C}_2\text{N}$), the thermodynamically most stable products of the reaction mechanism shown in Figure 1.

A third possible reaction channel is the transposition of hydrogen from MIN2 to MIN3 through the transition state TS8 at $-173.9 \text{ kJ mol}^{-1}$ and the subsequent dissociation of MIN3 to P2 through the transition state TS6 at $-326.7 \text{ kJ mol}^{-1}$. The elimination of a hydrogen atom from MIN2 gives the final product by overcoming a barrier of $197.8 \text{ kJ mol}^{-1}$. In the corresponding transition state TS4 ($172.5 \text{ kJ mol}^{-1}$ below the AL), a π bond is being formed between the two carbon atoms. The P1 products, namely, cyanoketene and a hydrogen atom, are $201.1 \text{ kJ mol}^{-1}$ more stable than the reactants. Because the process is exothermic and the whole energy profile lies below the AL, our computations suggest that this pathway represents a plausible mechanism for the formation of cyanoketene in the ISM. The relative electronic energies of all of the stationary points obtained at the rDSD and junChS-F12 levels are reported in Table 1.

4. RATE CONSTANTS

To prove that the reaction mechanism proposed in this work could justify the formation of cyanoketene in the ISM, it is necessary to perform kinetic computations.

The rate constants as a function of the temperature for the products P1, P2, and P3 obtained for the reaction between HCCN and HCO are shown in Figure 3. The parameters of the corresponding Arrhenius–Kooij fits are collected in Table 2.

Inspection of the results reported in Figure 3 shows that the formation rate constant of P1 ranges between 6.8×10^{-11} and

Table 1. Anharmonic Zero-Point-Corrected Energies (kJ mol^{-1}) Relative to the Asymptotic Limit for All of the Species Involved in the Reaction Computed Using the Two Different Levels of Theory Discussed in Section 2^a

Species	rDSD	junChS-F12
Rx1	0.0	0.0
MIN1	−190.4	−212.0
MIN2	−384.6	−370.3
MIN3	−381.9	−364.4
TS1	−102.6	−100.4
TS2	−143.6	−126.5
TS3	−50.2	−31.6
TS4	−193.7	−172.5
TS6	−338.7	−326.7
TS7	−189.1	−170.2
TS8	−194.2	−173.9
P1	−227.7	−201.1
P2	−382.5	−373.8
P3	−127.4	−114.1

^aThe RMS deviation of rDSD results from their junChS-F12 counterparts is 16.5 kJ mol^{-1} .

$1.22 \times 10^{-11} \text{ cm}^3 \text{ molecule}^{-1} \text{ s}^{-1}$ and is higher than the formation rate constants of P2 and P3 in the whole interval of temperatures (0–600 K). This is mainly due to the nature of the reaction pathways leading to P1, which includes the single-step path MIN2–TS4–P1, governed by one of the lowest activation energies of all of the reaction channels of MIN2 toward the possible products. The other single-step reaction pathway is MIN2–TS3–P2, and in this case, the very high activation energy (about 340 kJ mol^{-1}) makes it the most kinetically disfavored. All of the other pathways found by AutoMeKin involve multi-step reactions leading to the formation of P1, P2, and P3. Indeed, the second most competitive route is the transposition of hydrogen through MIN2–TS8–MIN3. Although TS8 is the lowest energy transition state, the multi-step nature of the corresponding reaction channel makes this route less favorable with respect to the MIN2–TS4–P1 pathway. P2 is the second most favored product because its formation rate constant takes values between 3.6×10^{-11} and $5.4 \times 10^{-11} \text{ cm}^3 \text{ molecule}^{-1} \text{ s}^{-1}$. Finally, the formation rate constant of P3 assumes values between 2.0×10^{-13} and $6.6 \times 10^{-13} \text{ cm}^3 \text{ molecule}^{-1} \text{ s}^{-1}$, which is the lowest of all the products of the reaction. This is probably due to the nature of the P3 formation pathway, which involves the highest activation barriers.

In summary, a detailed kinetic analysis shows that, despite the greater stability of P2 with respect to other possible products, cyanoketene is formed preferentially under the typical physical–chemical conditions of the ISM.

5. EXPERIMENT

5.1. Millimeter/Submillimeter-Wave Spectrometer.

The rotational spectrum of cyanoketene has been recorded by means of a millimeter/submillimeter-wave frequency-modulation spectrometer, described in detail elsewhere.^{75,76} Here, only a short summary is provided. A Gunn diode emitting in the W band (80–115 GHz) was used as primary source of radiation, whose frequency was locked *via* a phase-locked loop to a radio frequency local oscillator referenced to a 5 MHz rubidium atomic clock. Passive multipliers (doublers and triplers) were used in cascade to achieve spectral coverage

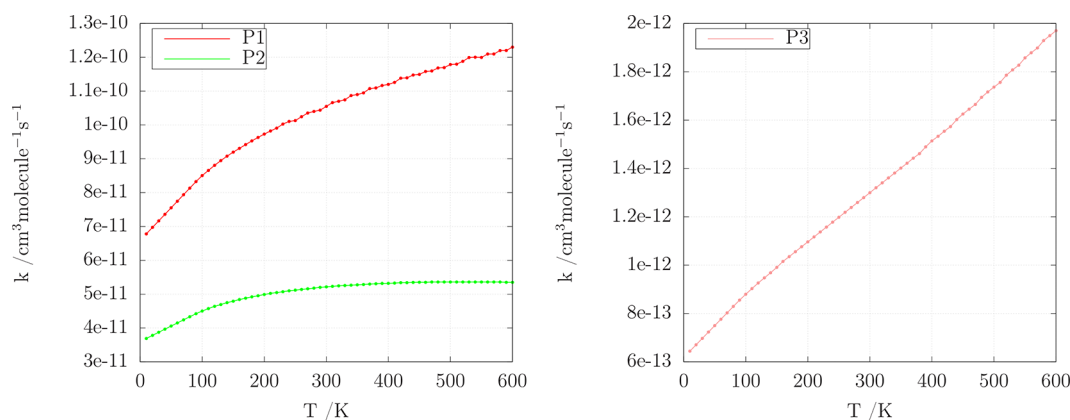


Figure 3. Temperature-dependence plots of the P1, P2 and P3 products of the HCCN + HCO reaction.

Table 2. Arrhenius–Kooij Parameters for the HCCN + HCO Reaction

	P1	P2	P3
A ($\text{cm}^3 \text{ molecule}^{-1} \text{ s}^{-1}$)	1.04×10^{-10}	5.48×10^{-11}	1.11×10^{-12}
n	0.22	0.02	0.68
E (kJ mol^{-1})	−44.60	132.46	−444.62
RMS ^a	2.90×10^{-13}	2.83×10^{-13}	1.86×10^{-14}

^aRMS stands for root-mean-square deviation of the fit.

at higher frequencies. The output radiation was sine-wave-modulated at $f = 48$ kHz and fed to the free-space glass absorption cell of the spectrometer, connected to the pyrolysis apparatus at one end and to a pumping system at the other end. Finally, the signal was detected by a liquid-He-cooled InSb hot electron bolometer (QMC Instruments, Ltd.) and demodulated by a lock-in amplifier set at twice the modulation frequency ($2f$), so that the second derivative of the actual spectrum was displayed. In this work, the uncertainty associated with our measurements ranges from 15 to 40 kHz depending upon the line width and the signal-to-noise ratio of the spectral line.

5.2. Production of Cyanoketene. As pointed out in previous papers,^{77,78} substituted ketenes can be formed via flash vacuum pyrolysis (FVP) of different precursors, namely, Meldrum's acid derivatives, isoxazolone compounds, or acetic acid derivatives. In the present work, cyanoketene was produced by the pyrolysis of gaseous methyl cyanoacetate ($\text{NCCH}_2\text{COOCH}_3$, 99% purity, Sigma-Aldrich) in the same apparatus previously employed for the study of other unstable molecules.^{79–82} The best yield of cyanoketene was attained by flowing the vapors of the precursor through a quartz tube heated at 1430 K by a tubular furnace. The pyrolysis products were continuously injected into the cell and subsequently pumped out from it, where the pressure was maintained at about 10 Pa.

No unexpected or unusually high safety hazards were encountered.

5.3. Spectrum Analysis and Results. Cyanoketene is a near-prolate asymmetric rotor ($\kappa = -0.98$) belonging to the C_s symmetry point group. All atoms lie in a plane defined by the two principal inertial axes a and b , and only two components, μ_a and μ_b , contribute to the total dipole moment $\mu = 3.542(15)$ D, with values of 2.844(12) and 2.112(9) D, respectively.⁸³ The rotational energies of cyanoketene can be derived using the standard semi-rigid Hamiltonian for an asymmetric rotor.

$$\mathcal{H} = \mathcal{H}_{\text{rot}} + \sum_n \mathcal{H}_{\text{cd}}^{(n\text{th})} \quad (1)$$

The rigid rotor part \mathcal{H}_{rot} contains the angular momentum operator \hat{J}^2 and its components

$$\mathcal{H}_{\text{rot}} = \frac{1}{2}(B + C)\hat{J}^2 + \left[A - \frac{1}{2}(B + C)\right]\hat{J}_z^2 + \frac{1}{2}(B - C)(\hat{J}_x^2 - \hat{J}_y^2) \quad (2)$$

where A , B , and C are the rotational constants and are related to the moments of inertia about the pertinent axes. The centrifugal distortion effects are recovered by adding several $\mathcal{H}_{\text{cd}}^{(n\text{th})}$ terms, up to the required power n . Here, the terms with $n = 4$ and 6 are expressed using the Watson-type S -reduced Hamiltonian in terms of the quartic (D and d) and sextic (H and h) centrifugal distortion constants.

$$\begin{aligned} \mathcal{H}_{\text{cd}}^S = & -D_J(\hat{J}^2)^2 - D_{JK}\hat{J}_z^2\hat{J}^2 - D_K\hat{J}_z^4 + d_J(\hat{J}_+^2 + \hat{J}_-^2) \\ & + d_2(\hat{J}_+^4 + \hat{J}_-^4) + H_J(\hat{J}^2)^3 + H_{JK}(\hat{J}^2)^2\hat{J}_z^2 \\ & + H_{KJ}\hat{J}_z^2\hat{J}^2 + H_K\hat{J}_z^6 + h_1(\hat{J}^2)(\hat{J}_+^2 + \hat{J}_-^2) + h_2 \\ & \hat{J}^2(\hat{J}_+^4 + \hat{J}_-^4) + h_3(\hat{J}_+^6 + \hat{J}_-^6) \end{aligned} \quad (3)$$

Higher order distortion terms have the general form⁸⁴

$$\mathcal{H}_{\text{cd}}^{(n\text{th})} = \sum_{i=0}^{n/2} X_i(\hat{J}^2)^{(n/2-i)}\hat{J}_z^{2i} + \sum_{i=1}^{n/2} x_i(\hat{J}^2)^{(n/2-i)}(\hat{J}_+^{2i} + \hat{J}_-^{2i}) \quad (4)$$

This work started when the spectroscopic parameters of NCCHCO were available only from Hahn et al.,⁸³ who investigated the microwave spectrum of cyanoketene below 40 GHz. Their set of constants were used to obtain an initial guess of the rotational spectrum above 80 GHz. By employing the

spectrometer described in section 5.1, a systematic search of the rotational transitions of cyanoketene was performed in selected frequency ranges between 80 and 530 GHz. A total number of 525 transitions (353 *a* type and 172 *b* type) have been recorded and analyzed, together with those observed by Hahn et al.,⁸³ in a weighted least squares procedure as implemented in the SPFIT/SPCAT suite of programs.⁸⁵

After the completion of this analysis, however, we became aware of the work published by Margulès et al.¹ Their study focused on the spectral region below 330 GHz and reported an extended analysis of several hundreds of *a*-type transitions, while the investigation of the *b*-type spectrum was more limited than in our work. Therefore, because of the different information brought by different types of transitions, we decided to perform a global fit of all of the available rotational transitions of cyanoketene, to further improve the accuracy of its spectroscopic parameters.

The determination of the complete set of octic centrifugal distortion constants is the major improvement achieved in our global fit. In particular, the determination of the L_K constant together with the accurate values obtained for several purely K_a -dependent centrifugal distortion parameters, such as D_K and H_K , is of great importance for predicting *b*-type $^{\prime}R$ transitions, whose intensity is the highest at any temperature up to 300 K.

The root-mean-square (RMS) error of the residuals of our analysis is 0.027 MHz, which is comparable to the accuracy of the experimental measurements, with the fit standard deviation (σ) being 0.90. A comparison of the final set of our spectroscopic parameters to those determined by Margulès et al.¹ is shown in Table 3.

A reformatted version of the FIT output file is provided in the Supporting Information. The new set of spectroscopic parameters allows for the reproduction and prediction of the rotational spectrum of cyanoketene in a wide frequency range, up to the ALMA band 9. The newly predicted frequencies can assist future astronomical search for cyanoketene in a huge frequency range, because the uncertainty in the line positions is generally lower than the typical spectral resolution of radio telescopes working in the millimeter/submillimeter domain.

6. DISCUSSION AND CONCLUSION

In this work, we have proposed a new formation route for cyanoketene involving two species already detected in the ISM, namely, the formyl and cyanocarbene radicals. The doublet potential energy surface starting from those reactants has been examined by an accurate yet feasible computational approach combining last-generation density functionals and composite wave function methods. To help the astronomical search of this molecule, we also carried out laboratory measurements of its rotational spectrum up to 530 GHz.

Because the results of our theoretical kinetic analysis support the conclusion that cyanoketene can be formed from HCO and HCCN by means of a hydrogen elimination reaction, we suggest to search for cyanoketene in the ISM regions where HCO and HCCN have been already detected. Unfortunately, to the best of our knowledge, those two radicals have been never detected in the same interstellar region. Anyway, the regions where at least one of those molecules has been detected are W3, NGC2024, W51, K3-50, IRC + 2016, and TMC-1. Among them, only TMC-1 has been investigated by Margulès et al.; therefore, we suggest to search for this molecule in the other aforementioned regions.

Table 3. Spectroscopic Parameters^a of Cyanoketene

Parameter	Present work	Margulès et al. ¹
<i>A</i>	29601.18220(77) ^a	29601.17783(98)
<i>B</i>	2812.149125(48)	2812.14944(11)
<i>C</i>	2563.721998(43)	2563.72222(11)
<i>D_J</i> × 10 ³	1.538791(19)	1.539026(76)
<i>D_{JK}</i> × 10 ³	−115.00852(48)	−115.00801(47)
<i>D_K</i> × 10 ³	2814.456(35)	2813.778(55)
<i>d₁</i> × 10 ⁶	−368.8083(61)	−368.8395(72)
<i>d₂</i> × 10 ⁶	−9.1506(18)	−9.1383(12)
<i>H_J</i> × 10 ⁶	0.0061426(35)	0.006213(22)
<i>H_{JK}</i> × 10 ⁶	−0.21744(15)	−0.21768(16)
<i>H_{KJ}</i> × 10 ⁶	−24.0662(27)	−24.0191(27)
<i>H_K</i> × 10 ⁶	834.52(61)	807.50(86)
<i>h₁</i> × 10 ⁹	2.3411(16)	2.3535(20)
<i>h₂</i> × 10 ⁹	0.13843(73)	0.13074(31)
<i>h₃</i> × 10 ⁹	0.04192(15)	0.04377(17)
<i>L_J</i> × 10 ¹²	−0.03119(23)	−0.0382(22)
<i>L_{JJK}</i> × 10 ¹²	1.431(15)	1.555(17)
<i>L_{JK}</i> × 10 ⁹	−0.03184(25)	−0.05033(14)
<i>L_{KJ}</i> × 10 ⁹	10.2005(95)	10.0790(97)
<i>L_K</i> × 10 ⁹	−315.6(32)	
<i>l₁</i> × 10 ¹⁵	−14.37(14)	−15.85(18)
<i>l₂</i> × 10 ¹⁵	−1.178(71)	
<i>l₃</i> × 10 ¹⁵	−0.704(28)	−1.17(38)
<i>l₄</i> × 10 ¹⁵	−0.0988(63)	−0.0579(7)
<i>P_{KJ}</i> × 10 ¹²	−3.353(10)	−3.206(10)
number of distinct lines	2050	
RMS (kHz)	27.0	
σ	0.90	

^aValues in parentheses are standard errors in units of the last quoted digits.

The second major outcome of this work is an improved set of spectroscopic constants, which can be used to refine the spectral predictions of cyanoketene from the microwave to the THz region. In particular, *b*-type transitions (which are expected to be bright across the whole spectrum) can be targeted with high precision and can be unequivocal proof of the presence of cyanoketene in spectral line surveys. High-mass star-forming regions represent the most suitable sources^{86,87} for performing future astronomical searches.

■ ASSOCIATED CONTENT

Supporting Information

The Supporting Information is available free of charge at <https://pubs.acs.org/doi/10.1021/acsearthspacechem.3c00060>.

Cartesian coordinates of all critical points, Mulliken charges and spin densities of all species involved in the reaction, reformatted version of the FIT output file, and the MESS input and output files (PDF)

■ AUTHOR INFORMATION

Corresponding Authors

Bernardo Ballotta — Scuola Normale Superiore, 56126 Pisa, Italy; orcid.org/0000-0002-1591-9189;

Email: bernardo.ballotta@sns.it

Luca Dore — Dipartimento di Chimica “Giacomo Ciamician”, Università di Bologna, 40126 Bologna, Italy; orcid.org/0000-0002-1009-7286; Email: luca.dore@unibo.it

Authors

Tainah D. Marforio – Dipartimento di Chimica “Giacomo Ciamician”, Università di Bologna, 40126 Bologna, Italy; orcid.org/0000-0003-0690-306X

Sergio Rampino – Dipartimento di Scienze Chimiche, Università degli Studi di Padova, 35131 Padova, Italy; Istituto Nazionale di Fisica Nucleare, Sezione di Pisa, 56127 Pisa, Italy; orcid.org/0000-0001-8525-7777

Emilio Martínez-Núñez – Departamento de Química Física, Facultade de Química, Campus Vida, Universidade de Santiago de Compostela, 15782 Santiago de Compostela, Spain; orcid.org/0000-0001-6221-4977

Vincenzo Barone – Scuola Normale Superiore, 56126 Pisa, Italy; orcid.org/0000-0001-6420-4107

Mattia Melosso – Dipartimento di Chimica “Giacomo Ciamician”, Università di Bologna, 40126 Bologna, Italy; orcid.org/0000-0002-6492-5921

Andrea Bottoni – Dipartimento di Chimica “Giacomo Ciamician”, Università di Bologna, 40126 Bologna, Italy; orcid.org/0000-0003-2966-4065

Complete contact information is available at:

<https://pubs.acs.org/10.1021/acsearthspacechem.3c00060>

Notes

The authors declare no competing financial interest.

ACKNOWLEDGMENTS

This work has been supported in Bologna and Pisa by MIUR “PRIN 2015” funds [Project “STARS in the CAOS (Simulation Tools for Astrochemical Reactivity and Spectroscopy in the Cyberinfrastructure for Astrochemical Organic Species)”, Grant 2015F59J3R] and the University of Bologna and Scuola Normale Superiore (RFO funds). This work was partially supported by the Consellería de Cultura, Educación e Ordenación Universitaria (Grupo de Referencia Competitiva ED431C 2021/40) and the Ministerio de Ciencia e Innovación through Grant PID2019-107307RB-I00.

REFERENCES

- (1) Margulès, L.; McGuire, B. A.; Motiyenko, R. A.; Brogan, C.; Hunter, T.; Remijan, A.; Guillemin, J. C. Millimeter Wave Spectroscopy of Cyanoketene (NC–CH=C=O) and an Observational Search in the ISM. *Astron. Astrophys.* **2020**, 638, A3.
- (2) Turner, B. E. Microwave Detection of Interstellar Ketene. *Astrophys. J. Lett.* **1977**, 213, L75–L79.
- (3) McGuire, B. A. 2018 Census of Interstellar, Circumstellar, Extragalactic, Protoplanetary Disk, and Exoplanetary Molecules. *Astrophys. J. Suppl. Ser.* **2018**, 239, 17.
- (4) Remijan, A. J.; Hollis, J.; Lovas, F.; Stork, W. D.; Jewell, P.; Meier, D. Detection of Interstellar Cyanoformaldehyde (CNCHO). *Astrophys. J. Lett.* **2008**, 675, L85.
- (5) Belloche, A.; Menten, K.; Comito, C.; Müller, H.; Schilke, P.; Ott, J.; Thorwirth, S.; Hieret, C. Detection of Amino Acetonitrile in Sgr B2(N). *Astron. Astrophys.* **2008**, 492, 769–773.
- (6) Melosso, M.; Belloche, A.; Martin-Drumel, M.-A.; Pirali, O.; Tamassia, F.; Bizzocchi, L.; Garrod, R.; Müller, H.; Menten, K.; Dore, L.; Puzzarini, C. Far-Infrared Laboratory Spectroscopy of Aminoacetonitrile and First Interstellar Detection of its Vibrationally Excited Transitions. *Astron. Astrophys.* **2020**, 641, A160.
- (7) McGuire, B. A.; Burkhardt, A. M.; Kalenskii, S.; Shingledecker, C. N.; Remijan, A. J.; Herbst, E.; McCarthy, M. C. Detection of the Aromatic Molecule Benzonitrile (c-C₆H₅CN) in the Interstellar Medium. *Science* **2018**, 359, 202–205.
- (8) Winnewisser, G.; Walmsley, C. The Detection of HC₃N and HC₇N in IRC + 10216. *Astron. Astrophys.* **1978**, 70, L37–L39.
- (9) Bizzocchi, L.; Tamassia, F.; Laas, J.; Giuliano, B. M.; Esposti, C. D.; Dore, L.; Melosso, M.; Canè, E.; Charmet, A. P.; Müller, H. S. P.; Spahn, H.; Belloche, A.; Caselli, P.; Menten, K. M.; Garrod, R. T. Rotational and High-Resolution Infrared Spectrum of HC₃N: Global Ro-vibrational Analysis and Improved Line Catalog for Astrophysical Observations. *Astrophys. J. Suppl. Ser.* **2017**, 233, 11.
- (10) Rivilla, V. M.; Colzi, L.; Fontani, F.; Melosso, M.; Caselli, P.; Bizzocchi, L.; Tamassia, F.; Dore, L. DC₃N Observations towards High-Mass Star-Forming Regions. *Mon. Not. R. Astron. Soc.* **2020**, 496, 1990–1999.
- (11) Loomis, R. A.; Burkhardt, A. M.; Shingledecker, C. N.; Charnley, S. B.; Cordiner, M. A.; Herbst, E.; Kalenskii, S.; Lee, K. L. K.; Willis, E. R.; Xue, C.; Remijan, A. J.; McCarthy, M. C.; McGuire, B. A. An Investigation of Spectral Line Stacking Techniques and Application to the Detection of HC₁₁N. *arXiv.org, e-Print Arch., Astrophys.* **2020**, arXiv:2009.11900.
- (12) Vazart, F.; Latouche, C.; Skouteris, D.; Balucani, N.; Barone, V. Cyanomethanimine Isomers in Cold Interstellar Clouds: Insights from Electronic Structure and Kinetic Calculations. *Astrophys. J.* **2015**, 810, 111.
- (13) Tonolo, F.; Lupi, J.; Puzzarini, C.; Barone, V. The Quest for a Plausible Formation Route of Formyl Cyanide in the Interstellar Medium: A State-of-the-Art Quantum-Chemical and Kinetic Approach. *Astrophys. J.* **2020**, 900, 85.
- (14) Zhang, W.; Du, B. Ab initio quantum chemical studies of reaction mechanism for CN with CH₂CO. *Int. J. Quantum Chem.* **2006**, 106, 1076–1085.
- (15) Sun, H.; He, H.-Q.; Hong, B.; Chang, Y.-F.; An, Z.; Wang, R.-S. Theoretical study of the mechanism of CH₂CO + CN reaction. *Int. J. Quantum Chem.* **2006**, 106, 894–905.
- (16) Edwards, M. A.; Herschberger, J. F. Kinetics of the CN+CH₂CO and NCO+CH₂CO reactions. *Chem. Phys.* **1998**, 234, 231–237.
- (17) Ballotta, B.; Nandi, S.; Barone, V.; Rampino, S. Gas-Phase Formation and Isomerization Reactions of Cyanoacetaldehyde, a Prebiotic Molecule of Astrochemical Interest. *ACS Earth Space Chem.* **2021**, 5, 1071–1082.
- (18) Xie, H. B.; Shi, G. S.; Ding, Y. H. Chemical Behavior of Polycyanoacetylene Radicals on Gaseous and Ice Water: A Computational Perspective. *Astrophys. J.* **2007**, 662, 758.
- (19) Xie, H. B.; Ding, Y. H.; Sun, C. C. Reaction Mechanism of Oxygen Atoms with Cyanoacetylene in the Gas Phase and on Water Ice. *Astrophys. J.* **2006**, 643, 573–581.
- (20) Xie, H. B.; Wang, J.; Zhang, S. W.; Ding, Y. H.; Sun, C. C. An ignored but most favorable channel for NCO+C₂H₂ reaction. *J. Chem. Phys.* **2006**, 125, 124317.
- (21) Guélin, M.; Cernicharo, J. Astronomical detection of the HCCN radical. Toward a new family of carbon-chain molecules? *Astron. Astrophys.* **1991**, 244, L21–L24.
- (22) Snyder, L.; Hollis, J.; Ulich, B. Radio detection of the interstellar formyl radical. *Astrophys. J.* **1976**, 208, L91–L94.
- (23) Alessandrini, S.; Barone, V.; Puzzarini, C. Extension of the “Cheap” Composite Approach to Noncovalent Interactions: The jun-ChS Scheme. *J. Chem. Theory. Comput.* **2020**, 16, 988–1006.
- (24) Güsten, R.; Wiesemeyer, H.; Neufeld, D.; Menten, K. M.; Graf, U. U.; Jacobs, K.; Klein, B.; Ricken, O.; Risacher, C.; Stutzki, J. Astrophysical Detection of the Helium Hydride Ion HeH⁺. *Nature* **2019**, 568, 357–359.
- (25) Melosso, M.; Bizzocchi, L.; Sipilä, O.; Giuliano, B.; Dore, L.; Tamassia, F.; Martin-Drumel, M.-A.; Pirali, O.; Redaelli, E.; Caselli, P. First Detection of NHD and ND₂ in the Interstellar Medium—Amidogen Deuteration in IRAS 16293-2422. *Astron. Astrophys.* **2020**, 641, A153.
- (26) Bacmann, A.; Faure, A.; Hily-Blant, P.; Kobayashi, K.; Ozeki, H.; Yamamoto, S.; Pagani, L.; Lique, F. Deuterium Fractionation of Nitrogen Hydrides: Detections of NHD and ND₂. *Mon. Not. R. Astron. Soc.* **2020**, 499, 1795–1804.
- (27) McGuire, B. A.; Brogan, C. L.; Hunter, T. R.; Remijan, A. J.; Blake, G. A.; Burkhardt, A. M.; Carroll, P. B.; van Dishoeck, E. F.; Garrod, R. T.; Linnartz, H.; Shingledecker, C. N.; Willis, E. R. First

Results of an ALMA Band 10 Spectral Line Survey of NGC 6334I: Detections of Glycolaldehyde ($\text{HC(O)CH}_2\text{OH}$) and a New Compact Bipolar Outflow in HDO and CS. *Astrophys. J. Lett.* **2018**, *863*, L35.

(28) Melosso, M.; Dore, L.; Tamassia, F.; Brogan, C. L.; Hunter, T. R.; McGuire, B. A. The Sub-millimeter Rotational Spectrum of Ethylene Glycol up to 890 GHz and Application to ALMA Band 10 Spectral Line Data of NGC 6334I. *J. Phys. Chem. A* **2020**, *124*, 240–246.

(29) Martínez-Núñez, E. An automated method to find transition states using chemical dynamics simulations. *J. Comput. Chem.* **2015**, *36*, 222–234.

(30) Martínez-Núñez, E. An automated transition state search using classical trajectories initialized at multiple minima. *Phys. Chem. Chem. Phys.* **2015**, *17*, 14912–14921.

(31) Martínez-Núñez, E.; Barnes, G. L.; Glowacki, D. R.; Kopec, S.; Peláez, D.; Rodríguez, A.; Rodríguez-Fernández, R.; Shannon, R. J.; Stewart, J. J. P.; Tahoces, P. G.; Vazquez, S. A. AutoMeKin2021: An open-source program for automated reaction discovery. *J. Comput. Chem.* **2021**, *42*, 2036–2048.

(32) Stewart, J. J. P. Optimization of parameters for semiempirical methods VI: More modifications to the NDDO approximations and re-optimization of parameters. *J. Mol. Model.* **2013**, *19*, 1–32.

(33) Stewart, J. J. P. *MOPAC2016*.

(34) Kozuch, S.; Martin, J. M. L. DSD-PBEP86: In search of the best double-hybrid DFT with spin-component scaled MP2 and dispersion corrections. *Phys. Chem. Chem. Phys.* **2011**, *13*, 20104–20107.

(35) Grimme, S.; Ehrlich, S.; Goerigk, L. Effect of the damping function in dispersion corrected density functional theory. *J. Comput. Chem.* **2011**, *32*, 1456–1465.

(36) Papajak, E.; Zheng, J.; Xu, X.; Leverentz, H. R.; Truhlar, D. G. Perspectives on Basis Sets Beautiful: Seasonal Plantings of Diffuse Basis Functions. *J. Chem. Theory Comput.* **2011**, *7*, 3027–3034.

(37) Biczysko, M.; Panek, P.; Scalmani, G.; Bloino, J.; Barone, V. Harmonic and Anharmonic Vibrational Frequency Calculations with the Double-Hybrid B2PLYP Method: Analytic Second Derivatives and Benchmark Studies. *J. Chem. Theory Comput.* **2010**, *6*, 2115–2125.

(38) Fukui, K. The path of chemical reactions—The IRC approach. *Acc. Chem. Res.* **1981**, *14*, 363–368.

(39) Garay-Ruiz, D.; Álvarez Moreno, M.; Bo, C.; Martínez-Núñez, E. New Tools for Taming Complex Reaction Networks: The Unimolecular Decomposition of Indole Revisited. *ACS Phys. Chem. Au* **2022**, *2*, 225–236.

(40) Raghavachari, K.; Trucks, G. W.; Pople, J. A.; Head-Gordon, M. A fifth-order perturbation comparison of electron correlation theories. *Chem. Phys. Lett.* **1989**, *157*, 479–483.

(41) Puzzarini, C.; Barone, V. Extending the Molecular Size in Accurate Quantum-Chemical Calculations: The Equilibrium Structure and Spectroscopic Properties of Uracil. *Phys. Chem. Chem. Phys.* **2011**, *13*, 7189–7197.

(42) Puzzarini, C.; Biczysko, M.; Barone, V.; Largo, L.; Peña, I.; Cabezas, C.; Alonso, J. L. Accurate Characterization of the Peptide Linkage in the Gas Phase: A Joint Quantum-Chemical and Rotational Spectroscopy Study of the Glycine Dipeptide Analogue. *J. Phys. Chem. Lett.* **2014**, *5*, 534–540.

(43) Barone, V.; Lupi, J.; Salta, Z.; Tasinato, N. Development and validation of a parameter-free model chemistry for the computation of reliable reaction rates. *J. Chem. Theory Comput.* **2021**, *17*, 4913–4928.

(44) Dunning, T. H. Gaussian basis sets for use in correlated molecular calculations. I. The atoms boron through neon and hydrogen. *J. Chem. Phys.* **1989**, *90*, 1007–1023.

(45) Woon, D. E.; Dunning, T. H. Gaussian basis sets for use in correlated molecular calculations. V. Core-valence basis sets for boron through neon. *J. Chem. Phys.* **1995**, *103*, 4572–4585.

(46) Papajak, E.; Zheng, J.; Xu, X.; Leverentz, H. R.; Truhlar, D. G. Perspectives on Basis Sets Beautiful: Seasonal Plantings of Diffuse Basis Functions. *J. Chem. Theory Comput.* **2011**, *7*, 3027–3034.

(47) Peterson, K. A.; Dunning, T. H. Accurate correlation consistent basis sets for molecular core-valence correlation effects: The second

row atoms Al–Ar, and the first row atoms B–Ne revisited. *J. Chem. Phys.* **2002**, *117*, 10548–10560.

(48) Möller, C.; Plesset, M. S. Note on an Approximation Treatment for Many-Electron Systems. *Phys. Rev.* **1934**, *46*, 618–622.

(49) Helgaker, T.; Klopper, W.; Koch, H.; Noga, J. Basis-set convergence of correlated calculations on water. *J. Chem. Phys.* **1997**, *106*, 9639–9646.

(50) Hill, J. G.; Mazumder, S.; Peterson, K. A. Correlation consistent basis sets for molecular core-valence effects with explicitly correlated wave functions: The atoms B–Ne and Al–Ar. *J. Chem. Phys.* **2010**, *132*, 054108.

(51) Werner, H.-J.; Adler, T. B.; Manby, F. R. General orbital invariant MP2-F12 theory. *J. Chem. Phys.* **2007**, *126*, 164102.

(52) Adler, T. B.; Knizia, G.; Werner, H.-J. A simple and efficient CCSD(T)-F12 approximation. *J. Chem. Phys.* **2007**, *127*, 221106.

(53) Lupi, J.; Alessandrini, S.; Barone, V.; Puzzarini, C. junChS and junChS-F12 Models: Parameter-free Efficient yet Accurate Composite Schemes for Energies and Structures of Noncovalent Complexes. *J. Chem. Theory Comput.* **2021**, *17*, 6974–6992.

(54) Barone, V.; Fusè, M.; Aguado, R.; Potenti, S.; León, I.; Alonso, E. R.; Mata, S.; Lazzari, F.; Mancini, G.; Spada, L.; Gualandi, A.; Cozzi, P. G.; Puzzarini, C.; Alonso, J. L. Bringing machine-learning enhanced quantum chemistry and microwave spectroscopy to conformational landscape exploration: The paradigmatic case of 4-fluoro-threonine. *Chem. - Eur. J.* **2023**, No. e202203990.

(55) Barone, V.; Di Grande, S.; Puzzarini, C. Toward accurate yet effective computations of rotational spectroscopy parameters for biomolecule building blocks. *Molecules* **2023**, *28*, 913.

(56) Bloino, J.; Biczysko, M.; Barone, V. General Perturbative Approach for Spectroscopy, Thermodynamics, and Kinetics: Methodological Background and Benchmark Studies. *J. Chem. Theory Comput.* **2012**, *8*, 1015–1036.

(57) Frisch, M. J.; Trucks, G. W.; Schlegel, H. B.; Scuseria, G. E.; Robb, M. A.; Cheeseman, J. R.; Scalmani, G.; Barone, V.; Petersson, G. A.; Nakatsuji, H.; Li, X.; Caricato, M.; Marenich, A.; Bloino, J.; Janesko, B. G.; Gomperts, R.; Mennucci, B.; Hratchian, H. P.; Ortiz, J. V.; Izmaylov, A. F.; Sonnenberg, J. L.; Williams-Young, D.; Ding, F.; Lipparini, F.; Egidi, F.; Goings, J.; Peng, B.; Petrone, A.; Henderson, T.; Ranasinghe, D.; Zakrzewski, V. G.; Gao, J.; Rega, N.; Zheng, G.; Liang, W.; Hada, M.; Ehara, M.; Toyota, K.; Fukuda, R.; Hasegawa, J.; Ishida, M.; Nakajima, T.; Honda, Y.; Kitao, O.; Nakai, H.; Vreven, T.; Throssell, K.; Montgomery, J. A., Jr.; Peralta, J. E.; Ogliaro, F.; Bearpark, M.; Heyd, J. J.; Brothers, E.; Kudin, K. N.; Staroverov, V. N.; Keith, T.; Kobayashi, R.; Normand, J.; Raghavachari, K.; Rendell, A.; Burant, J. C.; Iyengar, S. S.; Tomasi, J.; Cossi, M.; Millam, J. M.; Klene, M.; Adamo, C.; Cammi, R.; Ochterski, J. W.; Martin, R. L.; Morokuma, K.; Farkas, Ö.; Foresman, J. B.; Fox, D. J. *Gaussian 16, Revision C.01*; Gaussian, Inc.: Wallingford, CT, 2016.

(58) Werner, H.-J.; Knowles, P. J.; Knizia, G.; Manby, F. R.; Schütz, M. Molpro: A general-purpose quantum chemistry program package. *WIREs Comput. Mol. Sci.* **2012**, *2*, 242–253.

(59) Werner, H.-J.; Knowles, P. J.; Manby, F. R.; Black, J. A.; Doll, K.; Heßelmann, A.; Kats, D.; Köhn, A.; Korona, T.; Kreplin, D. A.; Ma, Q.; Miller, T. F.; Mitrushchenkov, A.; Peterson, K. A.; Polyak, I.; Rauhut, G.; Sibae, M. The Molpro quantum chemistry package. *J. Chem. Phys.* **2020**, *152*, 144107.

(60) Werner, H.-J.; et al. *MOLPRO, Version, a Package of Ab Initio Programs*.

(61) Georgievskii, Y.; Miller, J. A.; Burke, M. P.; Klippenstein, S. J. Reformulation and Solution of the Master Equation for Multiple-Well Chemical Reactions. *J. Phys. Chem. A* **2013**, *117*, 12146–12154.

(62) Tardy, D. C.; Rabinovitch, B. S. Collisional Energy Transfer. Thermal Unimolecular Systems in the Low-Pressure Region. *J. Chem. Phys.* **1966**, *45*, 3720–3730.

(63) Eckart, C. The Penetration of a Potential Barrier by Electrons. *Phys. Rev.* **1930**, *35*, 1303–1309.

(64) Pechukas, P.; Light, J. C. On Detailed Balancing and Statistical Theories of Chemical Kinetics. *J. Chem. Phys.* **1965**, *42*, 3281–3291.

- (65) Chesnavich, W. J. Multiple transition states in unimolecular reactions. *J. Chem. Phys.* **1986**, *84*, 2615–2619.
- (66) Fernández-Ramos, A.; Miller, J. A.; Klippenstein, S. J.; Truhlar, D. G. Modeling the Kinetics of Bimolecular Reactions. *Chem. Rev.* **2006**, *106*, 4518–4584.
- (67) Lupi, J.; Puzzarini, C.; Cavallotti, C.; Barone, V. State-of-the-Art Quantum Chemistry Meets Variable Reaction Coordinate Transition State Theory to Solve the Puzzling Case of the $\text{H}_2\text{S} + \text{Cl}$ System. *J. Chem. Theory Comput.* **2020**, *16*, 5090–5104.
- (68) Tsikritea, A.; Diprose, J. A.; Softley, T. P.; Heazlewood, B. R. Capture theory models: An overview of their development, experimental verification, and applications to ion–molecule reactions. *J. Chem. Phys.* **2022**, *157*, 060901.
- (69) Kooij, D. M. Über die Zersetzung des gasförmigen Phosphorwasserstoffs. *Z. Phys. Chem.* **1893**, *12U*, 155–161.
- (70) Laidler, K. J. A glossary of terms used in chemical kinetics, including reaction dynamics (IUPAC Recommendations 1996). *Pure Appl. Chem.* **1996**, *68*, 149–192.
- (71) Nandi, S.; Calderini, D.; Bloino, J.; Rampino, S.; Barone, V. A Modern-Fortran Program for Chemical Kinetics on Top of Anharmonic Vibrational Calculations. In *Computational Science and Its Applications—ICCSA 2019*; Misra, S., Gervasi, O., Murgante, B., Stankova, E., Korkhov, V., Torre, C., Rocha, A. M. A. C., Taniar, D., Apduhan, B. O., Tarantino, E., Eds.; Springer: Cham, Switzerland, 2019; Lecture Notes in Computer Science, Vol. 11624, pp 401–412, DOI: 10.1007/978-3-030-24311-1_29.
- (72) Nandi, S.; Ballotta, B.; Rampino, S.; Barone, V. A General User-Friendly Tool for Kinetic Calculations of Multi-Step Reactions within the Virtual Multifrequency Spectrometer Project. *Appl. Sci.* **2020**, *10*, 1872.
- (73) Balucani, N.; Skouteris, D.; Ceccarelli, C.; Codella, C.; Falcinelli, S.; Rosi, M. A theoretical investigation of the reaction between the amidogen, NH , and the ethyl, C_2H_5 , radicals: A possible gas-phase formation route of interstellar and planetary ethanimine. *Mol. Astrophys.* **2018**, *13*, 30–37.
- (74) Baiano, C.; Lupi, J.; Tasinato, N.; Puzzarini, C.; Barone, V. The Role of State-of-the-Art Quantum-Chemical Calculations in Astrochemistry: Formation Route and Spectroscopy of Ethanamine as a Paradigmatic Case. *Molecules* **2020**, *25*, 2873.
- (75) Melosso, M.; Conversazioni, B.; Degli Esposti, C.; Dore, L.; Cané, E.; Tamassia, F.; Bizzocchi, L. The Pure Rotational Spectrum of $^{15}\text{ND}_2$ Observed by Millimetre and Submillimetre-Wave Spectroscopy. *J. Quant. Spectrosc. Radiat. Transfer* **2019**, *222–223*, 186–189.
- (76) Melosso, M.; Bizzocchi, L.; Tamassia, F.; Degli Esposti, C.; Cané, E.; Dore, L. The Rotational Spectrum of ^{15}ND . Isotopic-Independent Dunham-Type Analysis of the Imidogen Radical. *Phys. Chem. Chem. Phys.* **2019**, *21*, 3564–3573.
- (77) Moloney, D.; Wong, M.; Flammang, R.; Wentrup, C. Cyanoketene and Iminopropadienones. *J. Org. Chem.* **1997**, *62*, 4240–4247.
- (78) Wentrup, C. Flash Vacuum Pyrolysis: Techniques and Reactions. *Angew. Chem., Int. Ed.* **2017**, *56*, 14808–14835.
- (79) Dore, L.; Bizzocchi, L.; Degli Esposti, C.; Gauss, J. The Magnetic Hyperfine Structure in the Rotational Spectrum of H_2CNH . *J. Mol. Spectrosc.* **2010**, *263*, 44–50.
- (80) Melosso, M.; McGuire, B. A.; Tamassia, F.; Degli Esposti, C.; Dore, L. Astronomical Search of Vinyl Alcohol Assisted by Submillimeter Spectroscopy. *ACS Earth Space Chem.* **2019**, *3*, 1189–1195.
- (81) Degli Esposti, C.; Melosso, M.; Bizzocchi, L.; Tamassia, F.; Dore, L. Determination of a Semi-Experimental Equilibrium Structure of 1-Phosphapropyne from Millimeter-Wave Spectroscopy of CH_3CP and CD_3CP . *J. Mol. Struct.* **2020**, *1203*, 127429.
- (82) Melli, A.; Potenti, S.; Melosso, M.; Herbers, S.; Spada, L.; Gualandi, A.; Lengsfeld, K. G.; Dore, L.; Buschmann, P.; Cozzi, P. G.; Grabow, J.-U.; Barone, V.; Puzzarini, C. A Journey from Thermally-Tunable Synthesis to Spectroscopy of Phenylmethanimine in Gas-Phase and Solution. *Chem. - Eur. J.* **2020**, *26*, 15016–15022.
- (83) Hahn, M.; Bodenseh, H.-K.; Ferner, M. Cyanoketene: The Microwave Spectrum and Structure of an Unstable Molecule. *J. Mol. Spectrosc.* **2004**, *223*, 138–147.
- (84) Gordy, W.; Cook, R. L. *Microwave Molecular Spectra*, 3rd ed.; Wiley: Hoboken, NJ, 1984.
- (85) Pickett, H. M. The Fitting and Prediction of Vibration-Rotation Spectra with Spin Interactions. *J. Mol. Spectrosc.* **1991**, *148*, 371–377.
- (86) Jørgensen, J. K.; Belloche, A.; Garrod, R. T. Astrochemistry During the Formation of Stars. *Annu. Rev. Astron. Astrophys.* **2020**, *58*, 727–778.
- (87) Coletta, A.; Fontani, F.; Rivilla, V.; Mininni, C.; Colzi, L.; Sánchez-Monge, A.; Beltrán, M. Evolutionary Study of Complex Organic Molecules in High-Mass Star-Forming Regions. *Astron. Astrophys.* **2020**, *641*, A54.